

## Disappearance of the Hexatic Phase in a Binary Mixture of Hard Disks

John Russo\*

*School of Mathematics, University of Bristol, Bristol BS8 1TW, United Kingdom*

Nigel B. Wilding†

*Department of Physics, University of Bath, Bath BA2 7AY, United Kingdom*

(Received 15 June 2017; published 14 September 2017)

Recent studies of melting in hard disks have confirmed the existence of a hexatic phase occurring in a narrow window of density which is separated from the isotropic liquid phase by a first-order transition, and from the solid phase by a continuous transition. However, little is known concerning the melting scenario in mixtures of hard disks. Here we employ tailored Monte Carlo simulations to elucidate the phase behavior of a system of large ( $l$ ) and small ( $s$ ) disks with diameter ratio  $\sigma_l/\sigma_s = 1.4$ . We find that as small disks are introduced to a system of large ones, the stability window of the hexatic phase shrinks progressively until the line of continuous transitions terminates at an end point beyond which melting becomes a first-order liquid-solid transition. This occurs at surprisingly low concentrations of the small disks,  $c \lesssim 1\%$ , emphasizing the fragility of the hexatic phase. We speculate that the change to the melting scenario is a consequence of strong fractionation effects, the nature of which we elucidate.

DOI: 10.1103/PhysRevLett.119.115702

One of the most celebrated accomplishments of statistical mechanics is the progress in understanding the rich physics of phase transitions in two-dimensional (2D) systems. In particular, the melting of 2D solids has puzzled researchers for decades. Early theoretical considerations [1] seemed to rule out the existence of 2D crystals, and the celebrated Mermin–Wagner theorem [2,3] proved that short-range continuous potentials cannot possess long-range positional order [4]. However, these theories were in conflict with early simulation results for hard disks [5] which suggested the presence of a first-order phase transition between a liquid and a solid [5]. The early simulations established hard disks as a benchmark system for testing theories of 2D melting, and motivated [6] Kosterlitz and Thouless (KT) to develop the theory that now bears their name [7] (also independently found by Berezinskii [8]). Within the KT theory, a new type of 2D solid phase is proposed, having long-range orientational order and only quasilong range positional order, and whose melting involves the continuous unbinding of dislocation pairs. The phase that results from the KT transition mechanism was originally believed to be an isotropic liquid, but Nelson, Halperin [9,10], and Young [11] realized that the new phase retains quasilong range orientational order, and melts via a second KT transition involving the unbinding of dislocations into free disclinations. The intermediate phase was called the *hexatic* phase, and the scenario of melting via two continuous transitions is known as the KTHNY theory.

KTHNY theory is based on the assumption that the solid phase remains stable on decompression until the continuous dislocation unbinding transition. It does not exclude the

possibility that this transition is preempted by a first-order transition, as simulations at first seemed to suggest. The two competing scenarios were debated for decades, see, e.g., Refs. [12–16], until a new class of *event-chain* rejection-free algorithms was developed that allowed the simulation of large systems in the melting region [17]. This led to a surprising discovery [17]: the melting of hard disks occurs via a continuous KT transition between the solid and hexatic phase, and via a first-order transition between the hexatic and liquid phase [18]. The work has also been extended and generalized to soft potentials [19,20], to hard polygons [21], and to hard-sphere monolayers [22], where the findings were even verified experimentally for colloidal particles [23].

Hitherto, studies of 2D melting have focused almost exclusively on pure (i.e., single component) systems. However, many important materials are *mixtures* of different sized particles, and exhibit phase behavior that is richer than for pure systems. A specific question of fundamental interest is “what happens to the melting transition of pure hard disks when a low concentration of smaller hard disks is introduced?” This second species acts as a form of disorder, which can selectively favor one particular phase, and might change the nature of the transition [24,25]. Here we consider the melting scenario for such a binary mixture of hard disks. We choose the size ratio between large ( $l$ ) and small ( $s$ ) disks to be  $\sigma_l/\sigma_s = 1.4$ , which is large enough to constitute a significant perturbation, but small enough to ensure that the minority ( $s$ ) component is included substitutionally rather than interstitially in the solid. We define the concentration of small disks by  $c = N_s/(N_l + N_s)$ , with  $N_l$  and  $N_s$  the number of large and small disks, respectively.

In order to obtain accurate coexistence properties of mixtures, one needs to account carefully for fractionation effects, i.e., the different partitioning of species among the coexisting phases [26]. Open ensembles are particularly suited for this purpose. Here we utilize Monte Carlo (MC) simulation in the semi-grand canonical ensemble (SGCE), in which disks can change their species [27], controlled by a fugacity fraction  $\xi = f_s/(f_l + f_s)$ , with  $f_s$  and  $f_l$  the fugacities of the  $s$  and  $l$  disks, respectively. The value of  $\xi$  sets the overall concentration, which will generally differ from that of the individual phases. In order to accelerate local density and concentration fluctuations we implement the event-chain algorithm [17,28], as well as a position swap for randomly selected pairs of disks. In the regime of small  $c$  of interest here,  $\xi$  is  $\mathcal{O}(10^{-5})$  and for convenience we quote only its coefficient; e.g., we write  $\xi = 3$  instead of  $\xi = 3 \times 10^{-5}$ .

The disks occupy a periodic square box of side  $L$  which, in common with other lengths, we measure in units of  $\sigma_l$ . In order to study the effects of varying  $c$ , we selected 16 different values of  $\xi$  in the interval  $\xi \in [0, 40]$ . For each  $\xi$ , we scanned (in a stepwise fashion) the range of number density  $\rho = (N_s + N_l)/L^2$  over which melting occurs. Within a two-phase region these paths of constant  $\xi$  correspond to tie lines along which phase separation occurs at constant fugacity for each component. We measured the pressure  $P$  along each tie line to obtain the corresponding equation of state (EOS),  $P(\rho)$  as described in the Supplemental Material [29]. This was found to exhibit the typical van der Waals loop of a first-order phase transition in a finite-sized system [30], which for pure hard disks correspond to the liquid to hexatic transition

[17]. Application of the Maxwell construction permitted the determination of the coexisting densities that mark the termini of the tie line.

In order to locate the density of the KT transition separating the hexatic and solid phases, we extended to binary mixtures the methods of Ref. [17]. Specifically, for each  $\xi$  we computed the pair correlation function  $g(r)$  for a sequence of densities. The hexatic-solid transition is signaled by a crossover in the form of  $g(r)$  from exponential (hexatic order) to power-law (solid) behavior. Since the system can exhibit a very large correlation length, the accurate location of the crossover density requires simulations of considerable size and duration. Most of our studies were performed for  $N = N_s + N_l = 256^2$  particles, while  $N = 512^2$  was used for a selected number of fugacities in order to assess finite-size effects, the analysis of which is further discussed in the Supplemental Material [29]. Overall, our simulations consumed well over 100 years of single-core CPU time.

Figure 1(a) presents our measurements of the density-concentration phase diagram. Apparent is a first-order phase coexistence region delineated by coexistence state points connected by tie lines. Within this region, a lower density phase coexists with a higher density phase, the nature of which we now examine for moderate  $\xi$ . A snapshot inside the coexistence region at  $\xi = 15$  and  $\rho = 0.91$ , is displayed in Fig. 1(b) and shows small disks as unfilled circles, while large disks are colored according to the phase of the hexatic order parameter,  $\psi_6^j = \sum_k \exp(i6\theta_{jk})/n_j$ , where, for each disk  $j$ ,  $k$  is one of the  $n_j$  nearest neighbors (defined as the disks whose cells share one edge with  $j$  in the radical Voronoi tessellation),

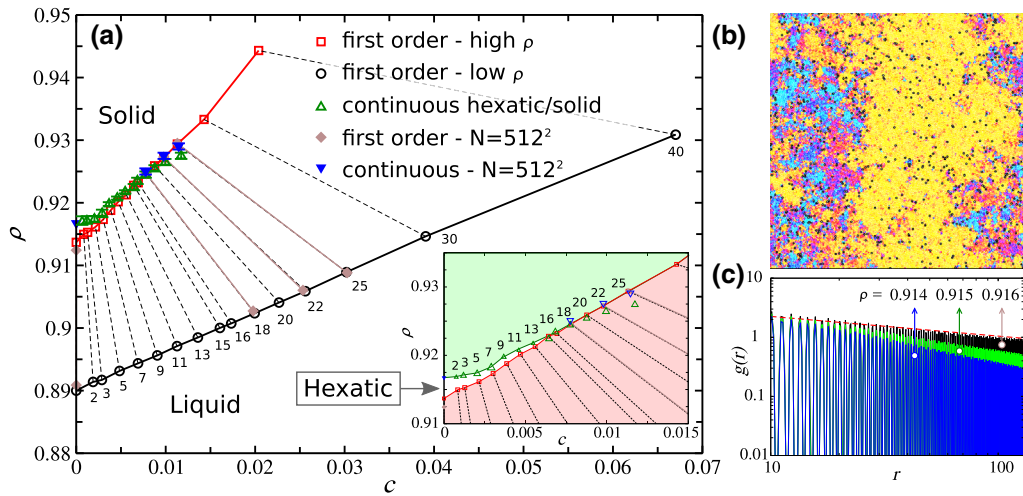


FIG. 1. (a) Phase diagram in the  $\rho$ - $c$  plane. Dashed tie lines connect first-order coexistence points for various  $\xi$  as marked. The line of continuous hexatic-solid transitions is shown as symbols, whose size is equal to the error bars (see the Supplemental Material [29]). Data correspond to  $N = 256^2$  unless otherwise indicated. The inset shows the region of low concentration. (b) Snapshot in the coexistence region at  $\xi = 15$  and  $\rho = 0.91$ . The color refers to the phase of the hexatic order parameter, while open circles are small disks plotted with twice their true size. (c)  $g(r) - 1$  (obtained as described in the Supplemental Material [29]) for  $\xi = 2$  at  $\rho = 0.914$  and  $0.915$  (hexatic phase), and  $\rho = 0.916$  (solid phase). The dashed line is the power-law scaling predicted by KTHNY theory.

and  $\theta_{jk}$  is the angle that the vector  $r_{jk}$  makes with a reference direction. Evident is a strip of dense phase having strong hexatic ordering, separated by a rough interface from a disordered (liquid) phase of lower density. The Supplemental Material [29] additionally shows that the EOS exhibits a loop. Both these properties are the hallmarks of a first-order phase transition. Figure 1(a) shows that on increasing  $c$ , the region of first-order coexistence (as found for the pure system in Ref. [17]) moves to higher  $\rho$  (and higher  $P$ ). Interestingly, as  $\xi$  increases, the slope of the tie lines rapidly flattens, implying that small disks are more easily “dissolved” in the disordered liquid phase. Our system thus behaves like a *eutectic* mixture [29].

Also indicated in Fig. 1(a) is the line of continuous hexatic-solid transitions, marked by the green and blue triangles, determined from the crossover in the form of  $g(r)$ . The nature of this crossover [29] is shown in Fig. 1(c) for state points spanning the transition line. The blue curve exhibits exponential decay (albeit with a very long correlation length) characteristic of the hexatic phase, while the black curve exhibits power-law decay characteristic of the 2D solid. The power-law exponent is compatible with  $-1/3$  (red dashed line), which corresponds to the predicted stability limit of the solid phase within KTHNY theory. Our results show that as small particles are introduced to the system, the continuous hexatic-solid transition point of the pure system becomes a line of KT transitions that extends to higher densities.

The inset of Fig. 1(a) expands the high density region of the phase diagram, revealing that as  $\xi$  is increased, the window of stability of the hexatic phase shrinks. For  $\xi = 20 \pm 2$ , corresponding to  $c \approx 1\%$ , the KT line *intersects*—and extends metastably into—the region of first-order coexistence. Thereafter, for  $\xi \gtrsim 20$ , the liquid phase coexists with a solid rather than a hexatic phase. Such an intersection point is analogous to the critical end point that features in the phase diagrams of many binary mixtures [31,32]. There a line of critical demixing transitions intersects and is truncated by a first-order transition line, the latter inheriting the singularities of the former. However, a difference between a critical end point and the end point in the present system is that the KT transition is of infinite-order within the classification scheme of Ehrenfest, and thus the free energy and all its derivatives are continuous. Accordingly, the locus of the first-order boundary in our system should be analytic.

In order to check for finite-size effects, we performed simulations with  $N = 512^2$  for  $\xi = 0, 18, 22, 25$ ; the results are included in Fig. 1(a). As in Ref. [17], the first-order coexistence window for the pure system narrows noticeably with increasing  $N$ , but this narrowing is much less pronounced at high  $\xi$  where the transition points are indistinguishable within our precision. The corresponding results for the KT line shift slightly to higher  $\rho$  with increased  $N$ , but the results still agree within uncertainty.

Overall, therefore, the  $N = 512^2$  results confirm the shrinking of the hexatic stability window.

Further evidence corroborating the disappearance of the hexatic phase can be gleaned from a study of the elastic constants of the solid phase. Specifically, we exploit KTHNY predictions for the Young’s modulus ( $K$ ) at the stability limit of the solid, to independently deduce the locus of the KT line. To estimate  $K$ , we measure both the shear and bulk moduli (see the Supplemental Material [29] and Refs. [33,34]). However, since the approach applies only to defect-free solids and is feasible only for much smaller  $N$  than considered above, we implement it in SGCE simulations of  $N = 3120$  disks in which defect generation is suppressed by the simple expedient of rejecting any update that would create a dislocation pair. In this way, measurements of  $K$  for the constrained (i.e., defect-free) solid, were made as a function of  $\rho$  for a number of values of  $\xi$ .

Of course, the equilibrium solid actually contains a nonzero population of defects, and, consequently, the measurements of  $K$  must be corrected to account for this. KTHNY theory [10] provides a framework for doing so which involves solving a set of renormalization group relations [34], starting from the  $K$  value of the defect-free solid. The solution also requires a calculation of the fugacity of dislocation pairs  $y$  (as described in the Supplemental Material [29]). The thus corrected values of  $K$  are plotted in Fig. 2(a) for various  $\xi$ . Note that KTHNY theory predicts the melting of the solid to occur when  $K/16\pi$  reaches unity under decompression, whereupon  $K$  jumps discontinuously to zero. Figure 2(a) thus shows that adding small disks softens the solid; i.e., it lowers  $K$ , resulting in an increase of the KT transition density.

Overall, the results emerging from Fig. 2(a) for the  $\xi$  dependence of the KT transition density are in good agreement with those shown in Fig. 1(a). Additionally,

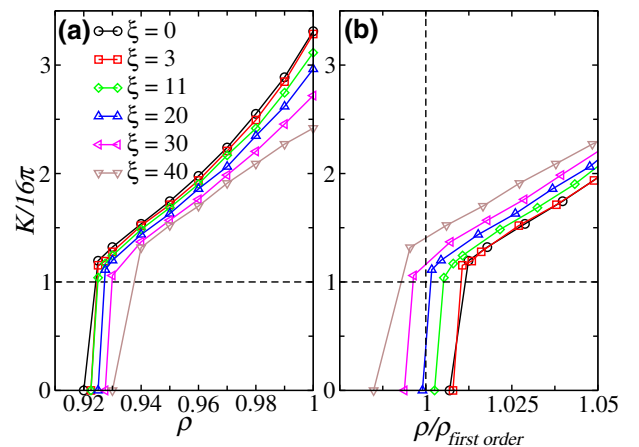


FIG. 2. (a) Normalized Young modulus ( $K/16\pi$ ) for various  $\xi$  as a function of  $\rho$ . The horizontal lines mark the stability limit  $K = 16\pi$  for the solid phase. (b) The same data plotted as a function of  $\rho/\rho_{\text{first order}}$  (see text).

the data for  $K(\rho)$  confirm the disappearance of the hexatic phase. This can be appreciated by replotting  $K$  as a function of  $\rho/\rho_{\text{first order}}$ , with  $\rho_{\text{first order}}$  the high density boundary of the first-order transition at each value of  $\xi$ . Represented in this way, the data [Fig. 2(b)] reveal that the shift of the KT transition to higher  $\rho$  with increasing  $\xi$  is *slower* than the shift of the first-order boundary, which therefore ultimately engulfs it. The value of  $\xi$  for which the KT line reaches its end point can be read off from Fig. 2(b) by locating that curve which intersects the point  $\rho/\rho_{\text{first order}} = 1, K/16\pi = 1$ . This occurs for  $\xi \cong 20$ , in accord with the previous estimate shown in Fig. 1(a).

We now attempt to rationalize the loss of the hexatic phase. Accordingly, we search for changes in the structural character of the phases on increasing  $\xi$  that might affect their entropy balance. We focus on three properties: (i) defect populations, (ii) spatial correlations between small particles, and (iii) degree of fractionation. Figure 3(a) plots the  $\rho$

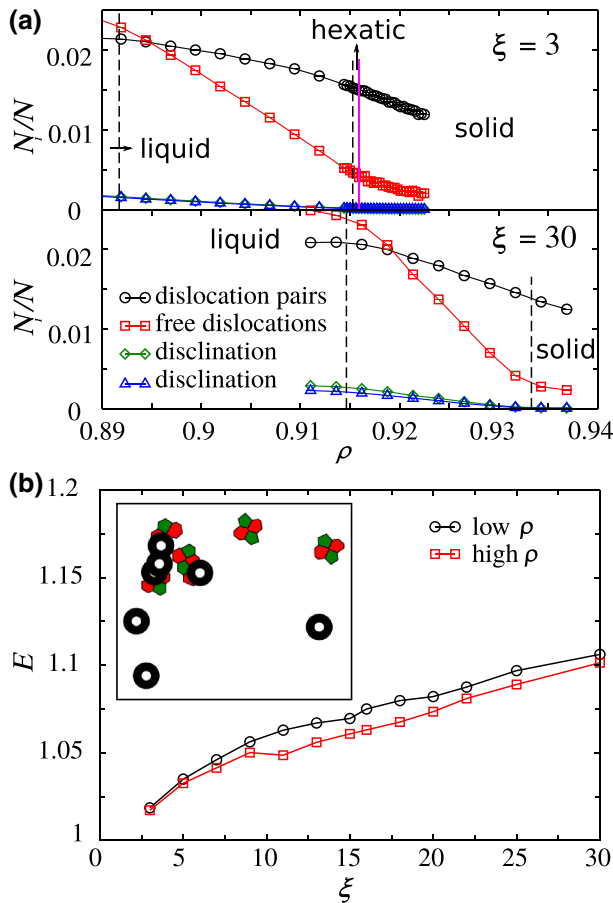


FIG. 3. (a) Fraction of sites with defects for  $\xi = 3$  and  $\xi = 30$ . The dashed vertical lines mark the boundaries of the first-order region. The purple vertical line marks the continuous transition. (b)  $\xi$  dependence of the evenness index ( $E$ ) at the low and high density boundary of the first-order region. Inset: snapshot of a small region at  $\xi = 30$  and  $\rho = 0.9343$  showing small disks (twice real size) and Voronoi cells for defects with 5 (green) and 7 (red) neighbors.

dependence of those defects relevant for the KTHNY transition; namely, 5–7 dislocation pairs, free 5–7 dislocations, and disclinations with 5 and 7 neighbors. Results are shown for  $\xi = 3$  and for  $\xi = 30$  [35]. Vertical dashed lines mark the coexistence boundary for the first-order transition, and for  $\xi = 3$  the purple line marks the density of the continuous transition. One observes that the KTHNY sequence of dislocation pairs (solid)  $\rightarrow$  free dislocations (hexatic)  $\rightarrow$  free disclinations (liquid) is obeyed for all  $\xi$  considered. One also notes that on traversing the phase transitions, the site fraction ( $N_i/N$ ) of all topological defects remains practically unchanged for both low and high  $\xi$  (see also Fig. S7 of the Supplemental Material [29]).

In order to assess how small particles are distributed, we plot in Fig. 3(b) their Pielou index ( $E$ ) as a function of  $\xi$  for densities on the low and high density boundary of the first-order region. This quantity measures the *evenness* of a distribution of points on a plane [36]:  $E = \pi\rho_s\bar{\omega}$ , where  $\rho_s$  is the density of small disks and  $\bar{\omega}$  is the average squared distance between a randomly chosen point on the plane and the nearest small disk.  $E = 1$  signifies a random distribution, while  $E > 1$  indicates clustering. As Fig. 3(b) shows, the value of  $E$  in both phases grows strongly with increasing  $\xi$ , indicating greater clustering. This is confirmed visually by snapshots [Fig. 3(b) and Fig. S7 of the SM [29]]. Interestingly, the two phases have a very similar  $E$  index for a given  $\xi$ , despite their very different values of  $c$  and degree of structural order. This latter result suggests that the contribution of small particle clustering to the entropy of the solid and liquid phase are rather similar. We also note in passing that small particle clusters tend to occur together with clusters of defects as shown in Fig. 3(b).

Taken together, these findings show that (i) the addition of small particles seems to have negligible effects on the population of defects at the transitions; (ii) there is little *difference* in the degree of small particle clustering between the phases (which might otherwise alter their entropy balance). Accordingly, it is not clear that the loss of the hexatic is attributable either to changes in defect populations or to particle clustering. Instead, we speculate that the effect is primarily driven by fractionation. Specifically, as  $\xi$  increases, the small particles migrate strongly to the liquid. This in turn raises the (mixing) entropy of the liquid compared to that of the hexatic or solid phases. The result is to stabilize the liquid relative to the higher density phase and hence to shift the first-order coexistence region to higher  $\rho$  faster than the KT line. Ultimately, then, the liquid region engulfs the hexatic, leaving only liquid-solid coexistence in its stead.

To conclude, we have investigated melting in a binary mixture of hard disks with  $\sigma_l/\sigma_s = 1.4$  as a function of the concentration of small particles. We have shown that the hexatic phase that occurs in the pure case survives only for very low  $c \lesssim 1\%$ , demonstrating that it is an utmost delicate

state of matter. For larger  $c$ , melting is a first-order transition directly from solid to liquid.

We thank H. Tanaka and R. Evans for helpful discussions. J. R. thanks the Royal Society for a URF fellowship, and the Blue Crystal supercomputer at the University of Bristol for a generous allocation of resources. Part of this research made use of the Balena High Performance Computing Service at the University of Bath.

---

\*john.russo@bristol.ac.uk  
†n.b.wilding@bath.ac.uk

- [1] R. E. Peierls, *Helv. Phys. Acta* **7**, 81 (1934).
- [2] N. D. Mermin and H. Wagner, *Phys. Rev. Lett.* **17**, 1133 (1966).
- [3] N. D. Mermin, *Phys. Rev.* **176**, 250 (1968).
- [4] P. Hohenberg, *Phys. Rev.* **158**, 383 (1967).
- [5] B. Alder and T. Wainwright, *Phys. Rev.* **127**, 359 (1962).
- [6] J. M. Kosterlitz, *Rep. Prog. Phys.* **79**, 026001 (2016).
- [7] J. Kosterlitz and D. Thouless, *J. Phys. C* **5**, L124 (1972).
- [8] V. Berezinskii, *Sov. Phys. JETP* **32**, 493 (1971).
- [9] B. I. Halperin and D. R. Nelson, *Phys. Rev. Lett.* **41**, 121 (1978).
- [10] D. R. Nelson and B. I. Halperin, *Phys. Rev. B* **19**, 2457 (1979).
- [11] A. Young, *Phys. Rev. B* **19**, 1855 (1979).
- [12] K. J. Strandburg, *Rev. Mod. Phys.* **60**, 161 (1988).
- [13] H. Weber, D. Marx, and K. Binder, *Phys. Rev. B* **51**, 14636 (1995).
- [14] J. Dash, *Rev. Mod. Phys.* **71**, 1737 (1999).
- [15] A. Jaster, *Phys. Rev. E* **59**, 2594 (1999).
- [16] C. Mak, *Phys. Rev. E* **73**, 065104 (2006).
- [17] E. P. Bernard and W. Krauth, *Phys. Rev. Lett.* **107**, 155704 (2011).
- [18] These findings have been verified by other methods: M. Engels, J. A. Anderson, S. C. Glotzer, M. Isobe, E. P. Bernard, and W. Krauth, *Phys. Rev. E* **87**, 042134 (2013).
- [19] S. C. Kapfer and W. Krauth, *Phys. Rev. Lett.* **114**, 035702 (2015).
- [20] M. Zu, J. Liu, H. Tong, and N. Xu, *Phys. Rev. Lett.* **117**, 085702 (2016).
- [21] J. A. Anderson, J. Antonaglia, J. A. Millan, M. Engel, and S. C. Glotzer, *Phys. Rev. X* **7**, 021001 (2017).
- [22] W. Qi, A. P. Gantapara, and M. Dijkstra, *Soft Matter* **10**, 5449 (2014).
- [23] A. L. Thorneywork, J. L. Abbott, D. G. A. L. Aarts, and R. P. A. Dullens, *Phys. Rev. Lett.* **118**, 158001 (2017).
- [24] J. T. Kindt, *J. Chem. Phys.* **143**, 124109 (2015).
- [25] A. S.-Y. Sheu and S. A. Rice, *J. Chem. Phys.* **129**, 124511 (2008).
- [26] N. B. Wilding and P. Sollich, *J. Chem. Phys.* **133**, 224102 (2010).
- [27] D. Frenkel and B. Smit, *Understanding Molecular Simulation* (Academic Press, New York, 2001), Vol. 1.
- [28] M. Michel, S. C. Kapfer, and W. Krauth, *J. Chem. Phys.* **140**, 054116 (2014).
- [29] See Supplemental Material at <http://link.aps.org/supplemental/10.1103/PhysRevLett.119.115702> for details of the determination of (a) the first order and KT lines, (b) fractionation effects, (c) elastic constant, (d) finite size effects, and (e) the wider phase diagram.
- [30] K. Binder, B. J. Block, P. Virnau, and A. Tröster, *Am. J. Phys.* **80**, 1099 (2012).
- [31] M. E. Fisher and P. J. Upton, *Phys. Rev. Lett.* **65**, 2402 (1990).
- [32] N. B. Wilding, *Phys. Rev. Lett.* **78**, 1488 (1997).
- [33] S. Sengupta, P. Nielaba, M. Rao, and K. Binder, *Phys. Rev. E* **61**, 1072 (2000).
- [34] S. Sengupta, P. Nielaba, and K. Binder, *Phys. Rev. E* **61**, 6294 (2000).
- [35] We consider only dislocation pairs of the smallest Burger's vector, as these are the most abundant at the densities considered.
- [36] E. C. Pielou, *J. Theor. Biol.* **13**, 131 (1966).